

Magnetic field evolution in simulations with Euler potentials

Axel Brandenburg^{1,2}

¹*NORDITA, AlbaNova University Center, Roslagstullsbacken 23, SE 10691 Stockholm, Sweden*

²*Department of Astronomy, AlbaNova University Center, Stockholm University, SE 10691 Stockholm, Sweden*

Revision : 1.36

ABSTRACT

Using two- and three-dimensional hydromagnetic simulations for a range of different flows, including laminar and turbulent ones, it is shown that solutions expressing the field in terms of Euler potentials (EP) are in general incorrect if the EP are evolved with an artificial diffusion term. In three dimensions, standard methods using the magnetic vector potential are found to permit dynamo action when the EP give decaying solutions. With an imposed field, the EP method yields excessive power at small scales. This effect is more exaggerated in the dynamic case, suggesting an unrealistically reduced feedback from the Lorentz force. The EP approach agrees with standard methods only at early times when magnetic diffusivity did not have time to act. It is demonstrated that the usage of EP with even a small artificial magnetic diffusivity does not converge to a proper solution of hydromagnetic turbulence. The source of this disagreement is not connected with magnetic helicity or the three-dimensionality of the magnetic field, but is simply due to the fact that the nonlinear representation of the magnetic field in terms of EP that depend on the same coordinates is incompatible with the linear diffusion operator in the induction equation.

Key words: magnetic fields — MHD — hydrodynamics – turbulence

1 INTRODUCTION

In the past few decades magnetic fields have become an integral part of many branches of observational and theoretical astrophysics. This is because in virtually all astrophysical bodies the electrical conductivity is large enough to support electric currents and hence magnetic fields. Furthermore, virtually all astrophysical flows produce dynamo action allowing part of the kinetic energy to be channelled through the magnetic energy reservoir before it is being dissipated (see Brandenburg & Subramanian 2005, for a review). Simulating such flows on the computer can become a serious challenge, in particular if one wants to reach large magnetic Reynolds numbers and if one wants to represent huge density contrasts that are typical for self-gravitating centrifugally supported structures such as galaxies. The same challenge is met in cosmological simulations that describe the formation of galaxy clusters and even the formation of galaxies. Many such simulations have been performed using smoothed particle hydrodynamics (Dolag et al. 2002). Its Lagrangian nature is well suited for handling self-gravity (Monaghan 1992). However, incorporating magnetic fields into such simulations has proved challenging. A possible solution to this problem may be the use of Euler potentials (Price & Bate 2007; Rosswog & Price 2007, 2008).

On a number of occasions the use of Euler potentials (EP) has proved useful in astrophysics and magnetohydrodynamics (Sweet 1950; Dungey 1958; Stern 1970; Sakurai 1979; Yahalom & Lynden-Bell 2006). In this approach the magnetic field is written as

$$\mathbf{B} = \nabla\alpha \times \nabla\beta, \tag{1}$$

where α and β are the EP. Until recently, the use of EP has only been modestly popular, because the nonlinearity of such a representation of \mathbf{B} can lead to difficulties in representing arbitrary initial conditions. Furthermore, as pointed out by Moffatt (1978), magnetic fields with linked or knotted \mathbf{B} lines cannot be represented with single-valued differentiable EP. Another problem is that one has the evolution equations for α and β only in the ideal case, i.e. when the resistivity vanishes. In that case one has to solve just two simple advection equations,

$$D\alpha/Dt = 0 \quad \text{and} \quad D\beta/Dt = 0. \tag{2}$$

Here, $D/Dt = \partial/\partial t + \mathbf{U} \cdot \nabla$ is the advective derivative and \mathbf{U} is the velocity. In recent years the use of Euler potentials has become increasingly popular in SPH simulations, because the evolution equations for α and β imply that the values of α and β are simply kept fixed at all times. Several tests have suggested that the use of EP can be superior to solving for \mathbf{B} because of the difficulty in preserving $\nabla \cdot \mathbf{B} = 0$ in numerical simulations (Dolag & Stasyszyn 2008). Differences between the two results could therefore readily be explained in terms of $\nabla \cdot \mathbf{B}$ not being zero in the latter approach. However, this does not eliminate concerns about the correctness of solutions obtained with the EP method compared to other methods that also preserve $\nabla \cdot \mathbf{B} = 0$. One such method is to solve for the magnetic vector potential (A method). In this paper we compare the two methods for a range of different flows.

2 EULER POTENTIALS IN SIMULATIONS

Kotarba et al. (2009) discussed the fact that the magnetic helicity vanishes in the EP representation, and so it is clear that this method is not well suited for studying helical or α effect dynamos that tend to produce magnetic fields with finite magnetic helicity. However, we still do not know what the magnetic field will be in such a case, and whether the EP method can still be useful for studying other types of dynamos, or at least other types of turbulent magnetohydrodynamic (MHD) flows.

The goal of this paper is to compare the evolution of the magnetic field in simulations using the EP method on the one hand and the magnetic vector potential method (A method) on the other. We do this by solving the equations for both methods at the same time. Of course, in the majority of cases, sharp gradients may develop eventually. This is when numerical methods for solving the equations of *ideal* MHD break down. It has then been customary to include artificial diffusion in the evolution equations for α and β , i.e. one considers solutions of the equations (Rosswog & Price 2007, 2008)

$$\frac{D\alpha}{Dt} = \eta \nabla^2 \alpha, \quad \frac{D\beta}{Dt} = \eta \nabla^2 \beta, \quad (3)$$

where η is the magnetic diffusivity. In the two-dimensional case with $\mathbf{B} = \mathbf{B}(x, y)$ and $B_z = 0$ we can write $\mathbf{B} = \nabla \times (A_z \hat{\mathbf{z}})$, where $\hat{\mathbf{z}}$ is the unit vector in the z direction, and A_z obeys the uncurled induction equation, which can be written as

$$\frac{DA_z}{Dt} = \eta \nabla^2 A_z. \quad (4)$$

To compare with the EP method, we choose $\beta = z$ and write $\mathbf{A} = \alpha \nabla \beta = \alpha \hat{\mathbf{z}}$, where $\hat{\mathbf{z}}$ is the unit vector in the z direction, so we have $A_z = \alpha(x, y, t)$, and thus the evolution equation for α becomes identical to that for A_z , even when $\eta \neq 0$. One can also write $\mathbf{A} = -\beta \nabla \alpha$, which agrees with the previous formulation after adding the gradient of $\alpha\beta$, which does not affect the \mathbf{B} field.

In order to facilitate direct comparison between the EP and A methods, we solve numerically Equation (3) together with the equation for the A method (Appendix A),

$$\frac{D\mathbf{A}}{Dt} = -\mathbf{A} \cdot (\nabla \mathbf{U})^T + \eta \nabla^2 \mathbf{A}, \quad (5)$$

where we have assumed $\eta = \text{const}$. We emphasize that the velocity \mathbf{U} enters Equations (3) and (5) also through the D/Dt derivative, and that the equations for both approaches are equivalent in the special case of $\eta = 0$. Indeed, if we insert a symmetrized representation,

$$\mathbf{A} = \frac{1}{2}(\alpha \nabla \beta - \beta \nabla \alpha) \quad (6)$$

into Equation (5), we obtain

$$\left(\frac{D\alpha}{Dt} - \eta \nabla^2 \alpha \right) \nabla \beta - \left(\frac{D\beta}{Dt} - \eta \nabla^2 \beta \right) \nabla \alpha = \mathbf{R} + \nabla \phi, \quad (7)$$

where \mathbf{R} stands for a residual term, and ϕ is given by

$$\phi = \frac{1}{2}(\alpha \dot{\beta} - \beta \dot{\alpha}) + \frac{1}{2}\nu(\alpha \nabla^2 \beta - \beta \nabla^2 \alpha) - \mathbf{U} \cdot \mathbf{A}. \quad (8)$$

The \mathbf{R} term vanishes for $\eta = 0$, but is finite with magnetic diffusivity and is then given by

$$\mathbf{R} = \eta(\nabla \alpha \cdot \nabla) \nabla \beta - \eta(\nabla \beta \cdot \nabla) \nabla \alpha. \quad (9)$$

Note that the $\nabla \phi$ term can be removed from Equation (7) by a gauge transformation; see Appendix B for the derivation. However, the \mathbf{R} term cannot be removed and, moreover, it has the same highest order of derivatives as the terms on the LHS of Equation (7),

so \mathbf{R} is in general not small. This is exactly the reason why the introduction of artificial diffusion is in general not permissible. The hope is, of course, that in the limit $\eta \rightarrow 0$ the EP and A methods give still reasonably similar results. In order to illustrate when this is the case, we consider in the following different flow fields.

3 CHOICE OF FLOW FIELDS

We first consider the case where \mathbf{U} is a given function and turn then to the case where \mathbf{U} is obtained by solving the momentum and continuity equations. In the former case we restrict ourselves to flows of the form

$$\mathbf{U} = \nabla \times \psi \hat{\mathbf{z}} + \phi \hat{\mathbf{z}}, \quad (10)$$

where $\psi = \psi(x, y, t)$ and $\phi = \phi(x, y, t)$ are prescribed functions that will be defined below. In the latter case we consider the compressible equations with an isothermal equation of state, so the density ρ is proportional to the pressure, which is then given by $p = \rho c_s^2$, where $c_s = \text{const}$ is the isothermal speed of sound. The governing equations are then

$$\frac{D \ln \rho}{Dt} = -\nabla \cdot \mathbf{U}, \quad (11)$$

$$\frac{D\mathbf{U}}{Dt} = -c_s^2 \nabla \ln \rho + \mathbf{f} + \mathbf{F}_{\text{visc}}, \quad (12)$$

where $\mathbf{F}_{\text{visc}} = \rho^{-1} \nabla \cdot 2\rho\nu\mathbf{S}$ is the viscous force, ν is the kinematic viscosity, $\mathbf{S}_{ij} = \frac{1}{2}(U_{i,j} + U_{j,i}) - \frac{1}{3}\delta_{ij} \nabla \cdot \mathbf{U}$ is the traceless rate of strain tensor, and \mathbf{f} is a nonhelical random forcing function consisting of plane transversal waves with random wavevectors \mathbf{k} such that $|\mathbf{k}|$ lies in a band around a given forcing wavenumber k_f (Haugen et al. 2004). The vector \mathbf{k} changes randomly from one timestep to the next. The forcing amplitude is chosen such that the Mach number $\text{Ma} = u_{\text{rms}}/c_s$ is about 0.1.

The total system of equations consists of Equations (3) and (5) together with Equations (11) and (12). In all cases the magnetic field is considered infinitesimally weak, so that the Lorentz force can be neglected. These equations were solved using the PENCIL CODE¹ which is a high-order finite-difference code (sixth order in space and third order in time) for solving the compressible MHD equations. The code came with a routine that solves two passive advection–diffusion equations that were invoked by compiling with `CHIRAL=chiral`, which is a routine that was originally designed for another purpose to describe the spontaneous chiral symmetry breaking in biomolecules (Brandenburg & Multamäki 2004). Additional diagnostics for monitoring the magnetic field and the current density have been added to this module for the purpose of this paper.

Initial conditions are generated by setting first α and β , and then calculating \mathbf{A} from Equation (6). We consider cubic domains of size L^3 using triply-periodic boundary conditions in all cases, except the first one which is a two-dimensional case where we assume perfect conductor boundary conditions. In either case, the magnetic helicity, $H = \int \mathbf{A} \cdot \mathbf{B} dV$, is gauge invariant, i.e. the transformation $\mathbf{A} \rightarrow \mathbf{A}' + \nabla \Lambda$ does not change the value of H . This is because

$$\int \nabla \Lambda \cdot \mathbf{B} dV = \oint \Lambda \mathbf{B} \cdot d\mathbf{S} - \int \Lambda \nabla \cdot \mathbf{B} dV \quad (13)$$

¹ <http://pencil-code.googlecode.com/>

vanishes owing to the condition $\nabla \cdot \mathbf{B} = 0$, and there is no surface term for periodic domains or perfectly conducting boundaries. So, the statement that in the EP approach $\mathbf{A} \cdot \mathbf{B} = 0$ is merely a gauge condition (Stern 1970) does not change the fact that we always have $H = 0$. On the other hand, the current helicity, $\int \mathbf{J} \cdot \mathbf{B} dV$, can well take values different from zero, as has been utilized in the calculation of force-free equilibria (Sakurai 1979). In the A approach H can generally be different from zero. However, if $H = 0$ initially, then H can become different from zero only through resistivity. This is a consequence of periodic or perfectly conducting boundaries.

4 RESULTS

4.1 Wind-up by a two-dimensional eddy

We consider first the wind-up of an initially uniform magnetic field, $\mathbf{B} = B_0 \hat{x}$, or $\alpha = B_0 y$ and $\beta = z$ in the EP formulation. We choose a flow with a single eddy given by Equation (10), i.e.

$$\psi(r) = (U_0/k) \cos^4 kr, \quad \phi(r) = \epsilon U_0 \psi(r), \quad (14)$$

where $r^2 = x^2 + y^2$ in a domain $-L/2 \leq x, y \leq L/2$ and $k = \pi/L$. For $\epsilon = 0$, this flow was used earlier to compute the magnetic field evolution in ideal MHD (Brandenburg & Zweibel 1994), so we were able to compare our results with theirs in the ideal case.

We adopt perfect conductor boundary conditions, which corresponds to keeping the values of α and β on the boundaries equal to their initial values. However, it is advantageous to subtract out the linear gradients of $\alpha = \alpha_0 + \alpha_1$ and $\beta = \beta_0 + \beta_1$ and solve only for the departures α_1 and β_1 , whose values vanish on the boundaries. In our case the imposed gradient fields are $\alpha_0 = B_0 y$ and $\beta_0 = z$, so the relevant evolution equations are

$$\frac{D\alpha_1}{Dt} = -U_y B_0 + \eta \nabla^2 \alpha_1, \quad \frac{D\beta_1}{Dt} = -U_z + \eta \nabla^2 \beta_1. \quad (15)$$

The result is shown in Figure 1 for the ideal case, $\eta = 0$, with $\epsilon = 2/\pi$ and different resolution. One sees clearly that B_{rms} increases linearly with time while the current density $\mathbf{J} = \nabla \times \mathbf{B} / \mu_0$ (with μ_0 being the vacuum permeability) increases quadratically with time. In B_{rms} the differences between EP and A methods are small, which is why we plot in the second panel the maximum value of $|\mathbf{J}|$. Departures from the more accurate solutions obtained at the next higher resolution appears roughly at the same times, but are seen more clearly in J_{max} than in B_{rms} . The linear and quadratic scalings for \mathbf{B} and \mathbf{J} , respectively, are well reproduced by either method provided the resolution suffices to resolve the progressively finer structures as time goes on. Looking at the plot of J_{max} , one can conclude that one may need slightly more points with the EP method than with the A method.

For $\epsilon = 0$ the EP method gives correct results even in the case of finite magnetic diffusion, as expected based on the equivalence of the underlying equations in that case. This is connected with the fact that the flow is two-dimensional and confined to the plane only. However, when $\epsilon \neq 0$ we have $U_z(x, y) \neq 0$ and $B_z(x, y) \neq 0$, and hence $\beta_1 \neq 0$. In this case, the \mathbf{R} term is in general non-vanishing, and so Equations (3) and (15) are then no longer equivalent to Equation (5), even though the flow and the field depend only on two spatial coordinates. This is demonstrated in Figure 2, where we plot the time dependence of the current helicity, $\langle \mathbf{J} \cdot \mathbf{B} \rangle$, in runs with zero and finite values of η . Note the mutual departure of the two methods after some time when $\eta \neq 0$.

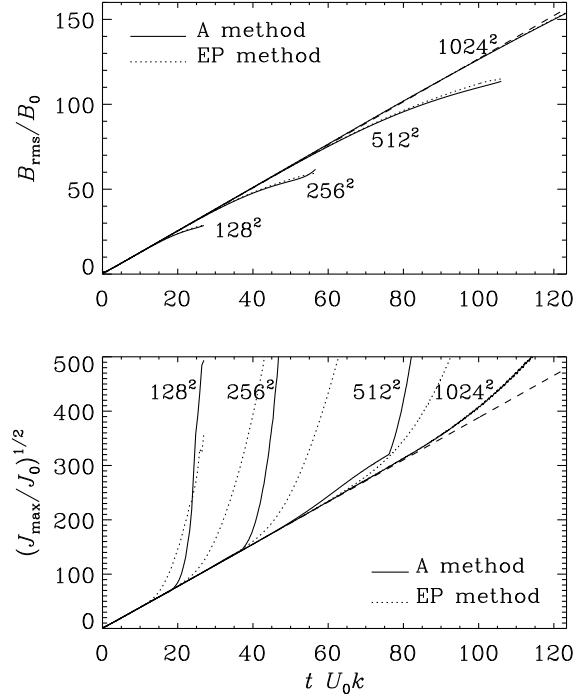


Figure 1. Evolution of B_{rms}/B_0 (upper panel) and $(J_{\text{max}}/J_0)^{1/2}$ (lower panel) for different resolutions with $\eta = 0$ and $\epsilon = 2/\pi$. Here, $J_0 = k B_0 / \mu_0$ has been used for normalization. In both plots dashed lines gives the ideal scalings, i.e. linear for \mathbf{B} and quadratic for \mathbf{J} .

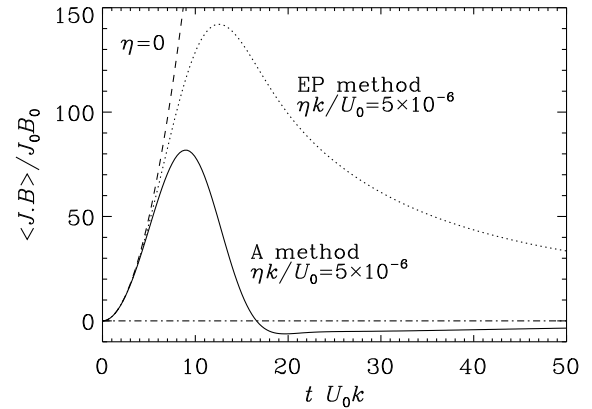


Figure 2. Evolution of the current helicity $\langle \mathbf{J} \cdot \mathbf{B} \rangle$ for $\epsilon = 2/\pi$ with $\eta = 0$ (where A and EP methods both give the same quadratic scaling; dashed line) and $\eta \neq 0$ (where the two methods disagree after some time). Again, $J_0 = k B_0 / \mu_0$ has been used for normalization.

These experiments have demonstrated that our implementation of the EP method along with the corresponding diagnostic tools give agreement with the A method, even when $\epsilon \neq 0$, provided $\eta = 0$. However, for $\eta \neq 0$ the two methods only agree when $\epsilon = 0$. It may appear that the disagreement is connected with the occurrence of current helicity, but this is not the case, as will be discussed at the end of the paper.

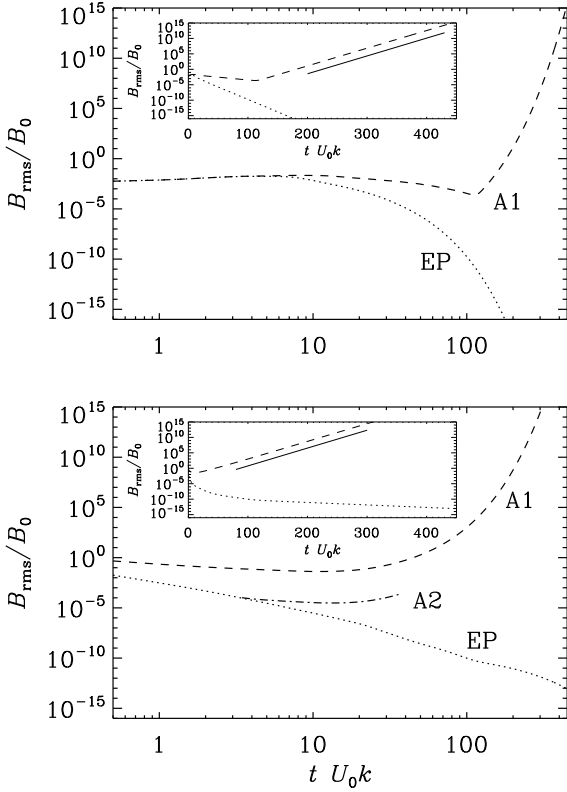


Figure 3. Comparison of the evolution of B_{rms} in a Roberts flow for methods A and EP for a smooth initial condition (upper panel) and a random one (lower panel) for resolution of 128^3 meshpoints and $R_m = U_0/\eta k = 200$. Both plots are double-logarithmic, so as to see more clearly the mutual departures of the two solutions at early times. The insets give the more usual linear-logarithmic representation showing clearly the exponential growth of the A solution at later times. The dash-dotted line departing from the EP line at $t = 3/U_0 k$ is the result of the A method, but with an initial condition calculated from the EP solution at that time (Run A2), as opposed to the initial time (Run A1).

4.2 Roberts flow dynamo

Next we discuss the Roberts (1972) flow given by Equation (10) with

$$\psi(x, y) = (U_0/k) \cos kx \cos ky, \quad \phi(x, y) = k_f \psi(x, y), \quad (16)$$

in the domain $-L/2 \leq x, y \leq L/2$, with $k = 2\pi/L$ and $k_f = \sqrt{2}k$. The Roberts flow is one of the simplest flows that produce dynamo action. The dynamo is however a slow one, i.e. its growth rate goes to zero in the limit $\eta \rightarrow 0$. The critical value of η is $\eta_{\text{crit}} = 0.181U_0/k$, so the critical value of the magnetic Reynolds number is $R_m = U_0 k/\eta_{\text{crit}} = 5.52$.

We have considered two different initial conditions, a smooth one given by $\alpha = \cos ky$ and $\beta = \cos kz$, and a random one where α and β are given by independent random functions. The results are shown in Figure 3. For smooth initial fields the EP and A methods agree up to 8 time units ($tU_0 k = 8$). This suggests that the EP method gives valid results only when magnetic diffusion did not yet have time to act. The A method shows that dynamo action commences after 100 time units, while the EP method gives only decaying solutions.

For random initial fields dynamo action occurs earlier, after about 10 time units, but the growth rate is the same as for smooth

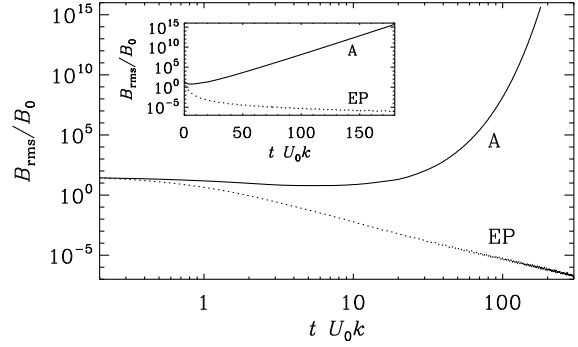


Figure 4. Comparison of the evolution of B_{rms} for the modified Galloway–Proctor flow with point-wise zero helicity for methods A and EP using 256^3 meshpoints and $R_m = 10^4$. Note the power law scaling for the EP method and the exponential scaling for the A method.

initial conditions. The reason for the difference in the onset of the exponential growth is that the eigenfunction of the dynamo mode overlaps poorly with the smooth initial condition, and does better so with random initial conditions. However, for random initial fields (with a spatially white noise power spectrum) the EP and A methods give different results from the very beginning (Runs A1 and EP). This is because of large discretization errors associated with the numerically different representations of white noise spectra. In order to check this we have calculated a new initial condition from the EP solution at time $t = 3/U_0 k$, when the field has become sufficiently smooth to be accurately represented by both methods. Now there is initial agreement, but it is still followed by a departure immediately afterwards (Run A2).

The results demonstrate quite clearly the difference with the EP method in handling helical dynamos, just as anticipated previously by Kotarba et al. (2009). However, it is still unclear whether the helical Roberts dynamo is just an exception, or whether the differences are of more general nature.

4.3 Flows with point-wise zero helicity

The problem with the Roberts flow is two-fold. Firstly, it is clear that the dynamo produces a large-scale field of Beltrami type and is therefore helical. This is impossible to represent in terms of EP. Secondly, the dynamo does not exist in the limit $\eta \rightarrow 0$, which is the only case where there is hope that the EP method can work. The latter problem could potentially be alleviated by choosing a flow that permits fast dynamos, where the growth rate remains finite in the limit $\eta \rightarrow 0$. However, this may not be true if $\eta \rightarrow 0$ is a singular limit, which is different from the case $\eta = 0$. Time-dependent flows of Galloway & Proctor (1992) type tend to be fast dynamos. An example of such a flow that has also point-wise zero kinetic helicity is given by (see Hughes et al. 1996)

$$\psi(x, y, t) = \sqrt{3/2}(U_0/k)[\cos kX(x, t) + \sin kY(y, t)], \quad (17)$$

$$\phi(x, y, t) = k \sin kX(x, t) \cos kY(y, t), \quad (18)$$

$$kX = kx + \cos \omega t, \quad kY = ky + \sin \omega t, \quad (19)$$

in the domain $-L/2 \leq x, y \leq L/2$, with $k = 2\pi/L$.

In Figure 4 we show an example for $R_m = U_0/\eta k = 10^4$. Again, it turns out that the EP method does not give solutions that are compatible with those of the A method. It turns that, while for the A method the field grows exponentially like $B_{\text{rms}} \sim e^{\lambda t}$, for

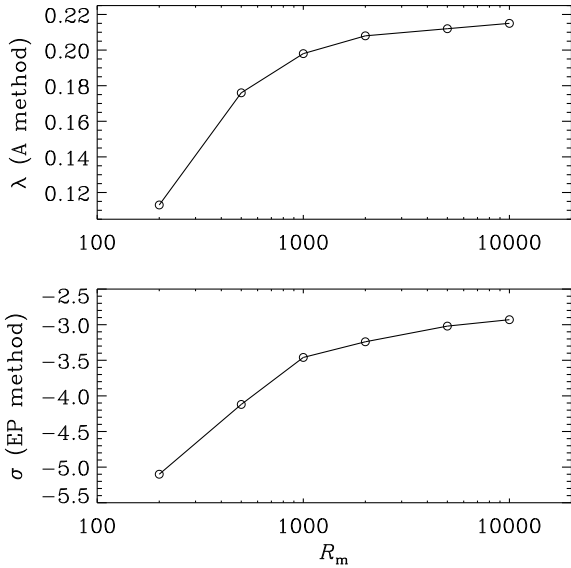


Figure 5. R_m dependence of the exponents λ and σ characterizing the evolution of $B_{\text{rms}} \sim e^{\lambda t}$ for the A method and $B_{\text{rms}} \sim t^\sigma$ for the EP method for the modified Galloway–Proctor flow with point-wise zero helicity for methods A and EP using 256^3 meshpoints.

the EP method the field decays algebraically like $B_{\text{rms}} \sim t^{-\sigma}$. In Figure 5 we plot the dependence of λ and σ on R_m . It turns out that λ seems to converge to a finite value (for the A method), and so does σ (for the EP method), confirming that the functional forms of the time dependencies for the A and EP methods are indeed different even for large values of R_m .

4.4 Nonhelically forced isotropic turbulence

The flows considered in Sections 4.2 and 4.3 are laminar. Another example of fast dynamo action, where the growth rate is comparable to the inverse turnover time, is isotropic turbulence. This is also the example that is closest to the application to turbulence in galaxy clusters. In that case there might be a chance to see a tendency toward dynamo action with the EP method when $\eta \rightarrow 0$. Unlike dynamos with helicity, we can only expect the magnetic field to have length scales smaller than the energy-carrying scale.

We consider here the case $k_f/k_1 = 3$, with $k_1 = 2\pi/L$ and a magnetic Reynolds number $R_m = u_{\text{rms}}/\eta k_f \approx 80$, using $\nu = \eta$. The result is shown in Figure 6. Just like in all previous cases, there is a stark difference in the evolution of the magnetic field computed with the A and EP methods. With the A method we reproduce exponential growth consistent with earlier findings in the literature (Cho & Vishniac 2000; Schekochihin et al. 2002; Haugen et al. 2003), while the EP method gives results that bear no resemblance with those where small-scale dynamo action is possible. The same is true of cross-sections of the field; see Figure 7. This strongly suggests that the EP method does not provide a solution that is close to the expected one, except for the case of a planar flow that depends only on two coordinates.

4.5 Spurious growth

In the early days of dynamo theory there have been cases of growing solutions that later turned out to be spurious due to lack of resolution. To demonstrate this in the present case, we present in

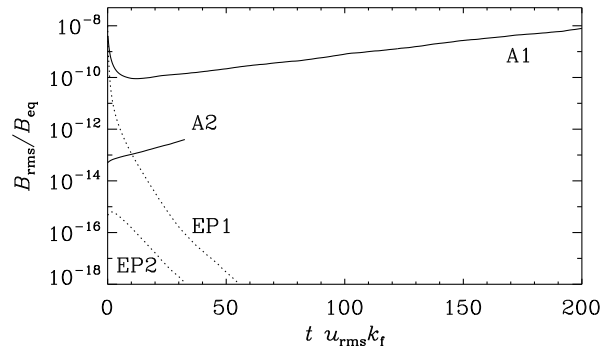


Figure 6. Comparison of the evolution of B_{rms} in nonhelical turbulence for methods A and EP using 128^3 meshpoints at $R_m = 80$ (Runs A1 and EP1) as well as $R_m = 160$ (Runs A2 and EP2). Note that the growth rate for Run A2 is slightly larger than that for A1, while the decay rates for EP1 and EP2 are the same.

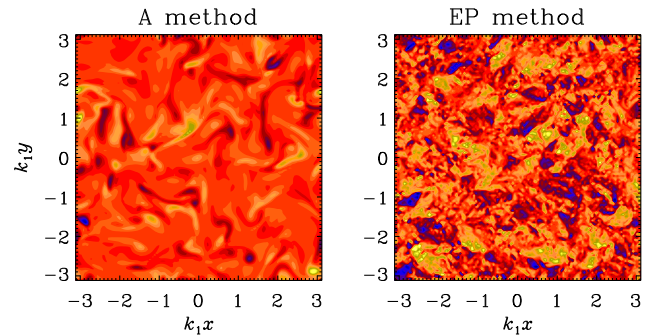


Figure 7. Comparison of cross-sections of $B_z(x, y)$ for methods A and EP from Runs A1 and EP1 after 200 time units, using 128^3 meshpoints at $R_m = 80$. Light (yellow) shades indicate positive values and dark (blue) shades indicate negative values. Note the absence of any resemblance between the two fields.

Figure 8 a solution with $\eta = 0$, keeping the fluid Reynolds number equal to 80, as in Figure 6.

The A and EP solutions show obvious signs of insufficient resolution with oscillation on the scale of the mesh. Nevertheless, both solutions show exponential growth with the same growth rate, which is spurious given the presence of oscillation on the mesh scale. This illustrates the importance of considering the dependence of the solutions on η , as was done in Section 4.4. In that case it turned out that the growth rate increases slightly with R_m , but this behavior was not reproduced by the EP method.

4.6 MHD turbulence with imposed field

The problems considered in Sections 4.2–4.5 had to do with dynamo action. This raises the question whether discrepancies between the A and EP methods also exist in other cases where there is no dynamo action. As an example we now consider nonhelical turbulence in the presence of an imposed field using $\alpha_0 = B_0 y$ and $\beta_0 = z$ as initial fields, similar what was done in Section 4.1. The energy density of the imposed field B_0 is comparable to the kinetic energy density. This is strong enough to dominate over dynamo action and may even suppress it. Here we choose the forcing

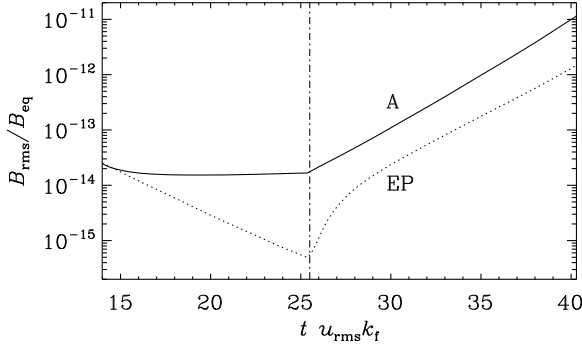


Figure 8. Spurious growth of B_{rms} to the right of the vertical line ($t u_{\text{rms}} k_f > 25.5$), for nonhelical turbulence and methods A and EP using 128^3 meshpoints with no resistivity ($\eta = 0$), and a fluid Reynolds number of 80.

wavenumber to be $k_f/k_1 = 1.5$. The fluid and magnetic Reynolds numbers are again around 80.

We consider both the kinematic case without feedback onto the flow and the dynamic case where the Lorentz force per unit mass, $\mathbf{J} \times \mathbf{B}/\rho$, has been added to the rhs of Equation (12) separately for the A and EP methods. The results are shown in Figure 9, where we plot magnetic power spectra for the two methods. It turns out that with the EP method, both the kinematic and dynamic cases yield excessive spectral magnetic energy at smaller scales (larger wavenumbers) compared to what the A method gives. Note also that with the EP method the resulting Lorentz force is weaker than with the A method, making the discrepancy even more pronounced in the dynamic case. With the A method kinetic and magnetic energy spectra are in approximate equipartition with each other, while with the EP method the magnetic field exceeds the spectral kinetic energy at progressively smaller scale.

5 DISCUSSION

Having demonstrated that under a number of circumstances of practical interest the EP method is unable to provide a meaningful trend when artificial diffusion is added, one wonders whether the source of this failure can be identified more precisely. In particular, we want to know whether this failure is connected with the inability to represent magnetic fields with helicity, or whether it is connected with the fact that the magnetic field is three-dimensional.

In order to address these issues, we consider now a simple decay problem with $\mathbf{U} = \mathbf{0}$ and look for solutions of the equations

$$\frac{\partial \mathbf{A}}{\partial t} = \eta \nabla^2 \mathbf{A}, \quad \text{or} \quad \frac{\partial \mathbf{B}}{\partial t} = \eta \nabla^2 \mathbf{B}, \quad (20)$$

that disagree with solutions of the equations

$$\frac{\partial \alpha}{\partial t} = \eta \nabla^2 \alpha, \quad \frac{\partial \beta}{\partial t} = \eta \nabla^2 \beta, \quad (21)$$

even though the initial conditions obey $\mathbf{B} = \nabla \alpha \times \nabla \beta$. The essence of the problem can already be demonstrated with a non-helical field in two dimensions. An example is

$$\alpha = -\cos ky, \quad \beta = \cos kx \sin ky, \quad (22)$$

which gives

$$\mathbf{B}(\mathbf{x}, 0) = (0, 0, k^2 \sin kx \sin^2 ky) \quad (23)$$

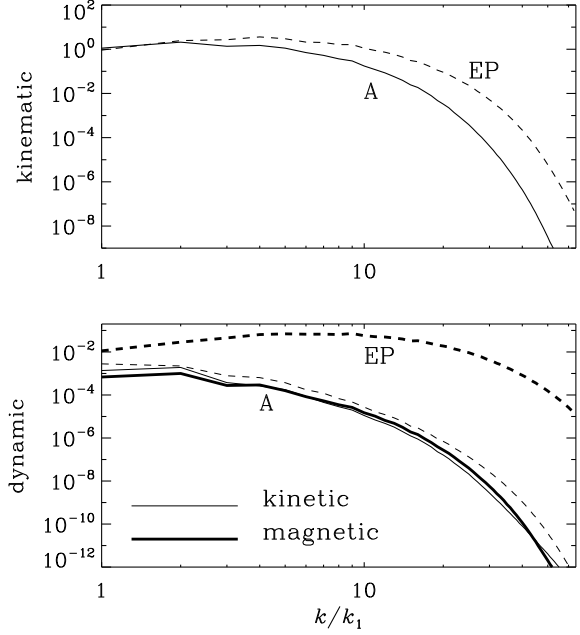


Figure 9. Magnetic power spectra for the kinematic case (upper panel) and the dynamic case (lower panel) for the A method (solid lines) and the EP method (dashed lines). In the dynamic case the kinetic energy spectra are also shown as thin solid and dashed lines for the A and EP methods. Here, $k_f/k_1 = 1.5$ and $R_m = 80$.

as initial field. Note that

$$\mu_0 \mathbf{J}(\mathbf{x}, 0) = (2 \sin kx \cos ky, -\cos kx \sin ky, 0) k \sin ky, \quad (24)$$

so $\mathbf{J} \cdot \mathbf{B} = 0$. With periodic boundary conditions, Equation (21) results in exponential decay of α and β while, owing to the non-linear representation of $\mathbf{B} = \nabla \alpha \times \nabla \beta$, the \mathbf{B} field shows a non-exponential decay; see Figure 10. This problem is also clear from the fact that the \mathbf{R} term in Equation (9) does not vanish. This is generally a consequence of α and β being simultaneously dependent on the same coordinates (in this case both α and β depend on y). Alternatively, if we choose $\alpha = \alpha(y)$ and $\beta = \beta(x)$ with

$$\alpha = \frac{1}{2} ky - \frac{1}{4} \sin 2ky, \quad \beta = \cos kx, \quad (25)$$

which also results in $\mathbf{B}(\mathbf{x}, 0)$ given by Equation (23), then $\mathbf{R} = \mathbf{0}$ and $\alpha(y, t)$ shows a non-exponential decay—compatible with the correct solution of $\mathbf{B}(\mathbf{x}, t)$.

In general, α and β are functions of all three coordinates, so the \mathbf{R} term in Equation (9) does not vanish and the EP method with artificial diffusion will give wrong results. Thus, we can say that the failure of the EP method in the presence of artificial diffusion is not related to magnetic helicity nor to the three-dimensionality of the magnetic field, but simply to the fact that the nonlinear representation of the magnetic field in terms of independent functions α and β is incompatible with the linear diffusion operator.

6 CONCLUSIONS

The EP method can give reliable results when $\eta = 0$, i.e. when one is interested in solutions to the ideal MHD equations. However, in practice this is not possible, especially when the flows are turbulent, because energy must be dissipated at the smallest scale. When one allows for magnetic diffusion to be present, there is no

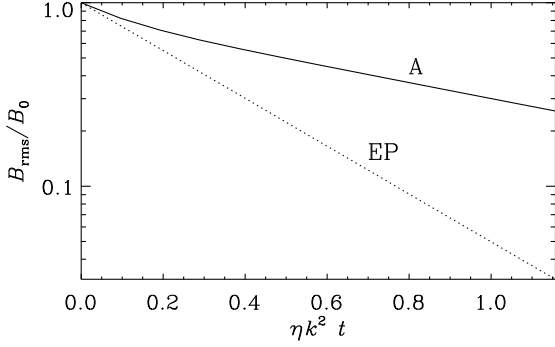


Figure 10. Decay of B_{rms} for solutions of Equations (20) and (21) using as initial conditions those given by Equations (22) and (23), respectively.

agreement between the EP and A methods. As a consequence, it is impossible to use the EP method to study dynamos. Even fast dynamos, which have finite growth rate in the limit $\eta \rightarrow 0$, cannot be modelled with the EP method. This means that any growth of the magnetic field found with the EP method cannot be due to dynamo action. This result is not just restricted to helical dynamos that can produce large-scale fields, but it also applies to nonhelical dynamos that produce small-scale fields.

Major discrepancies occur even in the case of an imposed field and in the absence of dynamo action. It is found that the EP method yields excessive spectral energy, in particular at small scales. This discrepancy becomes even more pronounced in the dynamic case owing to an apparent reduction of feedback from the Lorentz force compared with the A method. Indeed, the saturation strength of the magnetic field can be about 20 times larger with the EP method than with the A method.

In the ideal case, the A method may be slightly better suited to deal with limited numerical resolution than the EP method. However, once the resolution becomes insufficient, there can be cases where, in three dimensions, spurious exponential growth occurs with both methods. This underlines the necessity of diffusive processes, but with the EP method this inevitably leads to incorrect solutions.

One might expect that the A method gives good results also in Lagrangian schemes, because no derivative of \mathbf{A} needs to be computed. An exception is the diffusion term and, of course, the calculation of \mathbf{B} and \mathbf{J} for the Lorentz force (in full MHD) and for diagnostic purposes. The same is true for the EP method as well. It should therefore be worthwhile to explore the A method also in Lagrangian schemes.

ACKNOWLEDGMENTS

I thank Klaus Dolag, Hanna Kotarba, Daniel Price, and Federico Stasyszyn for discussions about the use of Euler potentials in SPH simulations, and Matthias Rheinhardt and Karl-Heinz Rädler for comments on the manuscript. I acknowledge the use of computing time at the Center for Parallel Computers at the Royal Institute of Technology in Sweden. This work was supported in part by the European Research Council under the AstroDyn Research Project 227952 and the Swedish Research Council grant 621-2007-4064.

REFERENCES

- Brandenburg A. 2001, ApJ, 550, 824
 Brandenburg A., Multamäki T. 2004, Int. J. Astrobiol., 3, 209
 Brandenburg A., Subramanian K. 2005, Phys. Rep., 417, 1
 Brandenburg A., Zweibel E. G. 1994, ApJ, 427, L91
 Dungey J. W. 1958, Cosmic Electrodynamics, CUP, Chap. 3
 Cho J., Vishniac E. 2000, ApJ, 538, 217
 Dolag K., Bartelmann M., Lesch H. 2002, A&A, 387, 383
 Dolag K., Stasyszyn F. A. 2008, arXiv:0807.3553
 Galloway D. J., Proctor M. R. E. 1992, Nature, 356, 691
 Haugen N. E. L., Brandenburg A., Dobler W. 2003, ApJ, 597, L141
 Haugen N. E. L., Brandenburg A., Dobler W. 2004, Phys. Rev. E, 70, 016308
 Hughes D. W., Cattaneo F., Kim E. J. 1996, Phys. Lett., 223, 167
 Kotarba H., Lesch H., Dolag K., Naab T., Johansson P. H., Stasyszyn F. A. 2009, MNRAS, 397, 733
 Moffatt H. K. 1978, Magnetic field generation in electrically conducting fluids (Cambridge University Press, Cambridge), Section 2.1.
 Monaghan J. J. 1992, ARA&A, 30, 543
 Price, D. J., Bate, M. R. 2007, MNRAS, 377, 77
 Roberts G. O. 1972, Phil. Trans. Roy. Soc. London A, 271, 411
 Rosswog, S.; Price, D. 2007, MNRAS, 379, 915
 Rosswog S., Price D. J., 2008, arXiv:0802.0418
 Sakurai T. 1979, Publ. Astron. Soc. Japan, 31, 209
 Schekochihin A. A., Maron J. L., Cowley S. C., McWilliams J. C. 2002, ApJ, 576, 806
 Stern, D. 1970, Am. J. Phys., 38, 494
 Sweet P. A. 1950, MNRAS, 110, 69
 Yahalom A., Lynden-Bell D., 2006, arXiv:physics/0603115

APPENDIX A: DERIVATION OF Equation (5)

For completeness we give here the derivation of Equation (5). The usual equation for \mathbf{A} is

$$\frac{\partial \mathbf{A}}{\partial t} = -\mathbf{E} - \nabla \phi, \quad (\text{A1})$$

where \mathbf{E} is the electric field and ϕ is the electrostatic potential. Using Ohm's law, $\mathbf{J} = \sigma(\mathbf{E} + \mathbf{U} \times \mathbf{B})$, as well as Ampere's law, $\mu_0 \mathbf{J} = \nabla \times \mathbf{B}$ and $\mathbf{B} = \nabla \times \mathbf{A}$ we have

$$\frac{\partial \mathbf{A}}{\partial t} = \mathbf{U} \times \nabla \times \mathbf{A} + \eta(\nabla^2 \mathbf{A} - \nabla \nabla \cdot \mathbf{A}) - \nabla \phi, \quad (\text{A2})$$

where we have dropped a term $(\nabla \cdot \mathbf{A})\nabla \eta$ on the RHS, because in our case $\eta = \text{const}$. Equation (A2) can be written as

$$\frac{\partial A_i}{\partial t} = -U_j \frac{\partial A_i}{\partial x_j} + U_j \frac{\partial A_j}{\partial x_i} + \eta \nabla^2 A_i - \nabla(\eta \nabla \cdot \mathbf{A} + \phi). \quad (\text{A3})$$

The first term on the RHS, together with the time derivative on the LHS, constitute the advective derivative, $D\mathbf{A}/Dt$. Next, we use

$$U_j \frac{\partial A_j}{\partial x_i} = -A_j \frac{\partial U_j}{\partial x_i} + \frac{\partial U_j A_j}{\partial x_i}, \quad (\text{A4})$$

so we have

$$\frac{D\mathbf{A}}{Dt} = -\mathbf{A} \cdot (\nabla \mathbf{U})^T + \eta \nabla^2 \mathbf{A} - \nabla(\eta \nabla \cdot \mathbf{A} - \mathbf{U} \cdot \mathbf{A} + \phi). \quad (\text{A5})$$

After a gauge transformation, $\mathbf{A} \rightarrow \mathbf{A}' + \nabla \Lambda$ with

$$\Lambda = \int_0^t (\eta \nabla \cdot \mathbf{A} - \mathbf{U} \cdot \mathbf{A} + \phi) dt' \quad (\text{A6})$$

we arrive at Equation (5).

APPENDIX B: DERIVATION OF EQUATION (8)

In order to verify the \mathbf{R} term in Equation (9) we calculate $\nabla^2 \mathbf{A}$ in terms of α and β , using $\mathbf{A} = \frac{1}{2}(\alpha \nabla \beta - \beta \nabla \alpha)$, so

$$\begin{aligned} A_{i,jj} &= \frac{1}{2}(\alpha_{,jj}\beta_{,i} - \beta_{,jj}\alpha_{,i}) + (\alpha_{,j}\beta_{,ij} - \beta_{,j}\alpha_{,ij}) \\ &+ \frac{1}{2}(\alpha\beta_{,ijj} - \beta\alpha_{,ijj}). \end{aligned} \quad (\text{B1})$$

Here, the last term in brackets can be written as the divergence of $\phi_1 = \frac{1}{2}(\alpha\beta_{,jj} - \beta\alpha_{,jj})$ minus $\frac{1}{2}(\alpha_{,i}\beta_{,jj} - \beta_{,i}\alpha_{,jj})$ which, in turn, is equal to the first term in Equation (B1), so we have

$$A_{i,jj} = (\alpha_{,jj}\beta_{,i} - \beta_{,jj}\alpha_{,i}) + (\alpha_{,j}\beta_{,ij} - \beta_{,j}\alpha_{,ij}) + \nabla_i \phi_1. \quad (\text{B2})$$

The first term in brackets corresponds to the diffusion terms in Equation (3), the second term explains the \mathbf{R} term in Equation (9), and ϕ_1 gives one of several terms entering in Equation (8).

For completeness let us here also give the derivation of the remaining terms. The time derivative of \mathbf{A} is given by

$$\begin{aligned} \frac{\partial A_i}{\partial t} &= \frac{1}{2}(\dot{\alpha}\beta_{,i} + \alpha\dot{\beta}_{,i} - \dot{\beta}\alpha_{,i} - \beta\dot{\alpha}_{,i}) \\ &= \dot{\alpha}\beta_{,i} - \dot{\beta}\alpha_{,i} + \frac{1}{2}\nabla_i(\alpha\dot{\beta} - \beta\dot{\alpha}), \end{aligned} \quad (\text{B3})$$

so we have

$$\frac{\partial \mathbf{A}}{\partial t} = \dot{\alpha} \nabla \beta - \dot{\beta} \nabla \alpha + \nabla \phi_2, \quad (\text{B4})$$

where $\phi_2 = \frac{1}{2}(\alpha\dot{\beta} - \beta\dot{\alpha})$, and dots denote partial time derivatives. Finally, from $\mathbf{U} \cdot \nabla \mathbf{A} + \mathbf{A} \cdot (\nabla \mathbf{U})^T$, we have in components form

$$U_j A_{i,j} + A_j U_{j,i} = U_j (A_{i,j} - A_{j,i}) - \nabla_i \phi_3, \quad (\text{B5})$$

where

$$A_{i,j} = \frac{1}{2}(\alpha\beta_{,ij} - \beta\alpha_{,ij}) + \frac{1}{2}(\alpha_{,j}\beta_{,i} - \beta_{,j}\alpha_{,i}), \quad (\text{B6})$$

and $\phi_3 = \mathbf{U} \cdot \mathbf{A}$. The first term in brackets of Equation (B6) is symmetric in i and j , while the second one is antisymmetric, so only the second one contributes to $A_{i,j} - A_{j,i}$, giving

$$\mathbf{U} \cdot \nabla \mathbf{A} + \mathbf{A} \cdot (\nabla \mathbf{U})^T = (\mathbf{U} \cdot \nabla \alpha) \nabla \beta - (\mathbf{U} \cdot \nabla \beta) \nabla \alpha - \nabla \phi_3.$$

The first two terms explain the advection operator in Equation (3), while the last term contributes to $\phi = \phi_1 + \phi_2 + \phi_3$ in Equation (8).